J. Fluid Mech. (1998), *vol.* 357, *pp.* 1–20. Printed in the United Kingdom

© 1998 Cambridge University Press

Binary collision of drops in simple shear flow by computer-assisted video optical microscopy

By S. GUIDO AND M. SIMEONE

Dipartimento di Ingegneria chimica, Università degli Studi di Napoli 'Federico II', Napoli 80125, Italy

(Received 15 January 1997 and in revised form 15 September 1997)

The collision of two equi-sized drops immersed in an immiscible liquid phase undergoing a shear flow in a parallel plate apparatus has been investigated over a range of capillary numbers. The drops were observed along the vorticity direction of shear flow by video enhanced contrast optical microscopy. Images of the colliding drops were processed by image analysis techniques. The distance Δy between the drop centres along the velocity gradient direction was measured as a function of time during approach, collision and separation of the two drops. It was found that Δy increases irreversibly after collision, thus providing a mechanism for drop dispersion in a concentrated system. Drop shape evolution during collision was characterized by measuring a deformation parameter and the angle made by the drop major axis with respect to the velocity gradient direction. The extent of the near-contact region when the drops are sliding on each other was also estimated. Coalescence was a rare event and was observed in the extensional quadrant of the shear flow. The experimental results show good agreement with numerical simulations recently reported in the literature.

1. Introduction

Polymer blending is a popular industrial practice to obtain materials with desired properties. The microscopic morphology of a polymer blend, which develops during processing and eventually becomes frozen in the final product, plays a fundamental role in determining material properties of industrial interest, such as mechanical strength and permeability. It is well known that morphology development under flow is mainly affected by two key phenomena, i.e. break-up and coalescence of the drops forming the dispersed phase.

While break-up involves a single drop and is not very influenced by the presence of neighbouring drops in a blend (Loewenberg & Hinch 1996*b*), coalescence is, by definition, the result of a many-particle interaction process. The first step of such a process is the approach and collision of two or more drops during flow. Subsequent stages are flattening of the surfaces of the colliding drops in the near-contact region, drainage of the intervening film of continuous phase and film rupture, leading to confluence. It is also well known that collisions do not always result in coalescence and that drop deformation tends to decrease the probability of coalescence (Chesters 1991).

Few experimental works have been aimed at a direct visualization of collision and coalescence of drops during flow. Mason and co-workers (Bartok & Mason 1959; Allan & Mason 1962; MacKay & Mason 1964) studied collisions of two or more drops under simple shear flow in a Couette apparatus, as an extension of earlier work on hydrodynamic interactions between rigid spheres and rods (Bartok & Mason 1957).

https://doi.org/10.1017/S0022112097007921 Published online by Cambridge University Press

These authors investigated also the effect of electric fields (Allan & Mason 1962) and the effect of diffusion of a component soluble in both phases (MacKay & Mason 1964) on coalescence under shear flow. Their work was mainly restricted to the case of quasi-spherical drops. By tracking the relative motion of two colliding drops, it was found that the distance between the centres of mass along the velocity gradient did not restore, after separation, to the value before collision, but became larger. The effect was predicted in a qualitative way by a model based on an expression for the force acting on the drops in the near-contact region derived from Jefferey's generalized theory for sheared rigid ellipsoids (Allan & Mason 1962). It was also suggested that the asymmetrical nature of drop collision provides a mechanism for diffusion of drops along the velocity gradient direction, i.e. across streamlines. Shear-induced self-diffusion of spherical particles has been observed experimentally only for rigid particles (Eckstein, Bailey & Shapiro 1977; Leighton & Acrivos 1987). The effect has been attributed to multi-body interactions, since binary collisions between spherical rigid particles do not produce a net cross-flow displacement. No experimental data are available in the literature on self-diffusion of drops in shear flow.

Recently, Loewenberg & Hinch (1996*a*, *b*) presented numerical simulations of sheared emulsions based on a boundary integral formulation to describe pairwise interactions between deformable drops. The efficient calculation procedure developed by these authors allowed them to circumvent the computational limitations of previous applications of the boundary integral method and to perform extensive simulations of concentrated emulsions on an ordinary workstation.

The calculation procedure was also applied to simulate the interaction of two colliding drops in an infinite medium under shear. Numerical simulations of binary collisions were performed over a range of values of the two fundamental parameters governing the motion of a drop in a sheared fluid: the viscosity ratio $\lambda = \mu_d/\mu_c$, where μ_c and μ_d are the viscosities of the continuous phase and of the drop, respectively, and the capillary number $Ca = \dot{\gamma} R \mu_c/\sigma$, where $\dot{\gamma}$ is the shear rate, R is the undeformed drop radius and σ is the interfacial tension. Results were obtained for the evolution of the following quantities during collision: the distance between the centres of mass along the velocity gradient, the deformation parameter D, defined as $(L-B)/(L+B)$, where L and B are, respectively, the major and minor axis of the deformed drop, the stress contribution of each drop to shear stress, and the first and second normal stress difference.

Such calculations provide a complete three-dimensional picture of drop collision under shear flow, both in terms of relative motion and of drop shape evolution. In particular, it was found that drop collision leads to drop dispersion along the velocity gradient, in agreement with Mason and the coworkers' experimental observations. Furthermore, it was shown that the deformation and shear stress contribution of the drops were maximal when the drops are pressed together in the compressional quadrant of the shear flow and minimal when they are drawn apart in the extensional quadrant. Drop coalescence was not observed in the simulations since modelling of interfacial phenomena, such as van der Waals attraction, was not included in the study. However, by using scaling arguments, it was predicted that for $Ca \ll 1$ or $\lambda \neq O(1)$ the tendency for coalescence is greatest when drops are pressed together by the shear flow. On the other hand, for viscosity ratios and Ca both of order one, the tendency for coalescence was predicted to be greatest when the drops are drawn apart in the extensional quadrant of shear flow (Loewenberg & Hinch 1996*b*).

Experimental results for a suitable comparison with Loewenberg & Hinch computer simulations appear to be lacking, especially for the case of drops significantly deformed

https://doi.org/10.1017/S0022112097007921 Published online by Cambridge University Press

by shear flow. In this article, we present a set of experimental data describing binary collisions of drops under simple shear flow in a parallel plate apparatus. Drop interaction was followed by direct visualization through video optical microscopy and studied in a quantitative way by image analysis techniques. Experimental conditions included neutrally buoyant and equi-sized drops, and Newtonian behaviour of both continuous and dispersed phase in the range of shear rates investigated. Experiments were performed at two viscosity ratios and at several values of Ca. The tendency of the drops to coalesce is a related issue for which only preliminary results will be presented. The experimental procedure is described in §2, results are presented in §3, and concluding remarks are given in §4.

2. Experimental

2.1. *Materials and shear apparatus*

The fluids used in this work are polyisobutylene (PIB) and polydimethylsiloxane (PDMS). In order to vary the viscosity ratio between drop and continuous phase, two PDMS samples of different molecular weight, which will be denoted as PDMS 100 and PDMS 200, were selected for the experiments. All the experiments were performed at ambient temperature (~ 25 °C). Both polymers are transparent and the difference between their refractive indices is high enough to have good optical contrast for observations.

The two polymers can be considered immiscible for practical purposes. However, careful observations revealed that drops of PIB (in the μm size) immersed in PDMS (either 100 or 200) experienced a slow decrease in diameter with time. On the contrary, no significant variation of size was observed for drops of either PDMS in PIB, even after a few days. These results were attributed to a small solubility of PIB in PDMS. Owing to the polydispersity of the PIB sample used in this work, it is expected that the diffusion of PIB from the drop in the PDMS continuous phase is selective, i.e. the lower molecular weight chains will diffuse out first. As a consequence, the viscosity ratio will increase with time, though slowly. Therefore, for higher precision, experiments to be analysed in a quantitative way were carried out by using PIB as the continuous phase and PDMS, either 100 or 200, as the drop phase. A few observations, for qualitative purposes, were also performed by inverting the phases, i.e. using PIB as the drop fluid.

Buoyancy effects are expected to be negligible owing to the small density difference ($0.08\ \mathrm{g\ cm^{-3}}$) and the high viscosity of the two polymers (the Newtonian plateau viscosities are 81 Pa.s for PIB, 109 Pa.s for PDMS 100 and 190 Pa.s for PDMS 200 at 25 °C). A quantitative criterion to evaluate buoyancy effects can be obtained by comparing the buoyancy-driven velocity $\Delta\rho g R^2/\mu_c$ and the shear velocity $\dot{\gamma}R$. In the experiments performed in this work the ratio between the two velocities is of the order of 10^{-3}, thus showing that buoyancy is indeed negligible.

For values of the shear rate $\dot{\gamma}$ below $1\ \mathrm{s^{-1}}$ the rheological behaviour of both PIB and PDMS can be considered as Newtonian to a good approximation, as indicated by (i) the constancy of viscosity with shear rate, and (ii) the negligible values of first normal stress difference and dynamical modulus G'. In all the experiments described in this work, the shear rate $\dot{\gamma}$ was set at about $0.1\ \mathrm{s^{-1}}$ or below, i.e. well within the Newtonian plateau of both polymers. However, when two sheared drops come into apparent contact, one could conceive that higher local values of shear rate can be attained in the intervening film of continuous phase. As a consequence, the fluid in the near contact region might display a viscoelastic behaviour. An estimate of the shear rate in the near

https://doi.org/10.1017/S0022112097007921 Published online by Cambridge University Press

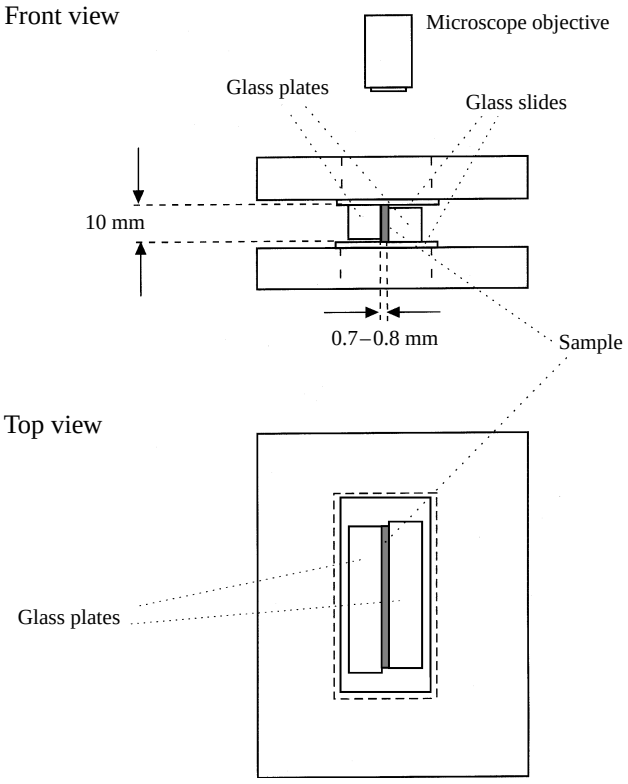


FIGURE 1. Schematic of parallel plates assembly.

contact region can be made by using the scaling arguments proposed by Loewenberg & Hinch (1996*b*). The local velocity in the near contact region can be written as $u = u_p + u_t$, where u_t is the tangential velocity on the drop interfaces and u_p is the velocity of pressure-driven flow. From scaling arguments, the rate of strain estimated from either velocity component is $u_p/h = u_t/c \approx R^2h/c^3$ (Loewenberg, private communication), where c is the radius of the near contact region and h is the thickness of the film between the two drops. For $Ca = O(1)$, $c \approx R$ and the highest rate of strain in the gap is $u_t/c = \dot{\gamma}R/h \ll \dot{\gamma}$. It can be concluded that non-Newtonian effects are not expected to affect the results of this work.

The interfacial tension for the PIB/PDMS system used in this work has been measured by Sigillo *et al.* (1997) through analysis of steady state drop deformation, drop retraction and thread break-up. By comparing the results obtained by these techniques, an average value of 3.0 ± 0.5 mN m^{-1} was obtained.

Simple shear flow was generated by a parallel plate apparatus. Both plates (100 mm × 10 mm × 10 mm) were made of glass and each one, as shown in figure 1, was glued on a glass slide (100 mm × 50 mm × 3 mm), which was, in turn, fit in a window cut on a rigid mount. One of the two mounts was screwed on an x, y-motorized stage equipped with two computer-controlled stepper motors (LEP Ltd), thus allowing the corresponding glass plate to be displaced with respect to the other along two perpendicular directions. Minimum and maximum motor speeds were 0.0084 mm s^{-1} and 30 mm s^{-1}, respectively. The maximum travel was 100 mm, with a positioning accuracy of 5 μm. The x- and y-directions of the motorized stage were used, respectively, to shear the sample and to set the gap between the glass plates.

https://doi.org/10.1017/S0022112097007921 Published online by Cambridge University Press

Adjustment of a micrometric tilting stage, as checked by a stage micrometer, guaranteed that the inner surface of the moving plate was being displaced in its own plane. Parallelism between the glass plates was adjusted through a set of translating, rotary and tilting stages by exploiting the reflections of a laser beam from the glass surfaces. The parallelism accuracy was of the order of 20 μm over the whole plate length of 100 mm. Typical gap values were between 0.7 and 0.8 mm, in order to minimize edge effects due to the confining surfaces of the two glass slides. To test apparatus performance, the velocity as a function of the distance from the fixed plate along the y-direction was measured by tracking the motion of small impurities or dust particles inside the sample. The velocity profiles obtained were linear, as expected for simple shear flow.

One of the main features of the experimental set-up was that the sheared sample could be observed by looking through the glass slides, i.e. along the vorticity axis of the shear flow. Observations were performed through a transmitted light microscope (Axioscop FS from Zeiss) equipped with a B/W CCD video camera (Hitachi KP-ME1) and a motorized focus system (LEP Ltd). The microscope itself was mounted on a motorized translating stage (Contek) in order to keep the sheared drops within the field of view during motion. The whole apparatus was placed on a vibration-isolated workstation (Newport).

The optics selected for the experiments included the following components (all from Zeiss): long working distance objectives (a $2.5\times/0.075$ Plan-Neofluar, a $10\times/0.25$ Achrostigmat, and a $20\times/0.40$ Achroplan), to allow focusing through the whole sample thickness; a brightfield condenser 0.9 Z; an additional lens holder (Optovar slider) which enabled the total magnification to be varied with factors of $1.25\times$ and $1.6\times$; and a zoom lens with a continuously adjustable zoom factor in the range 0.5–$2.0\times$.

2.2. *Drop formation*

The polymer selected as the continuous phase was loaded between the glass plates with the following procedure. Once alignment of the glass surfaces was completed, the moving plate was driven apart from the fixed one along the y-direction of the motorized stage. The polymer was then loaded between the two plates by a syringe. The moving plate was again brought towards the fixed plate along the y-axis until the desired gap was reached. The parallelism was rechecked by using the microscope to measure the gap thickness at several positions, to see if some misalignment was introduced by squeezing a viscous fluid between the two plates. It was also verified optically that the moving plate was still translating in its own plane. The small deviations found, if any, were then corrected by using the micrometric stages.

At this point, drops of the polymer selected as the dispersed phase were injected in the sample by a tiny glass capillary (o.d. was around 0.3 mm, with an inside diameter of about 0.1 mm). The glass capillary was introduced in the gap by a home-made micromanipulator. Care was taken to generate isolated drops at about half-way distance between the two glass slides along the y-direction in order to avoid edge effects. After injection of a few isolated drops in the sample, the capillary was gently extracted from the gap.

The next step was to generate two drops of about equal size to be used for a collision. This was achieved by breaking an isolated drop in two daughter drops. The sample was sheared at a capillary number above the critical value for drop break-up. To avoid formation of multiple satellites, the drop was not allowed to break up under shear, but the flow was stopped before growth of Rayleigh instabilities at the interface. If the drop was extended enough by the action of shear, it broke up during relaxation. The process

https://doi.org/10.1017/S0022112097007921 Published online by Cambridge University Press

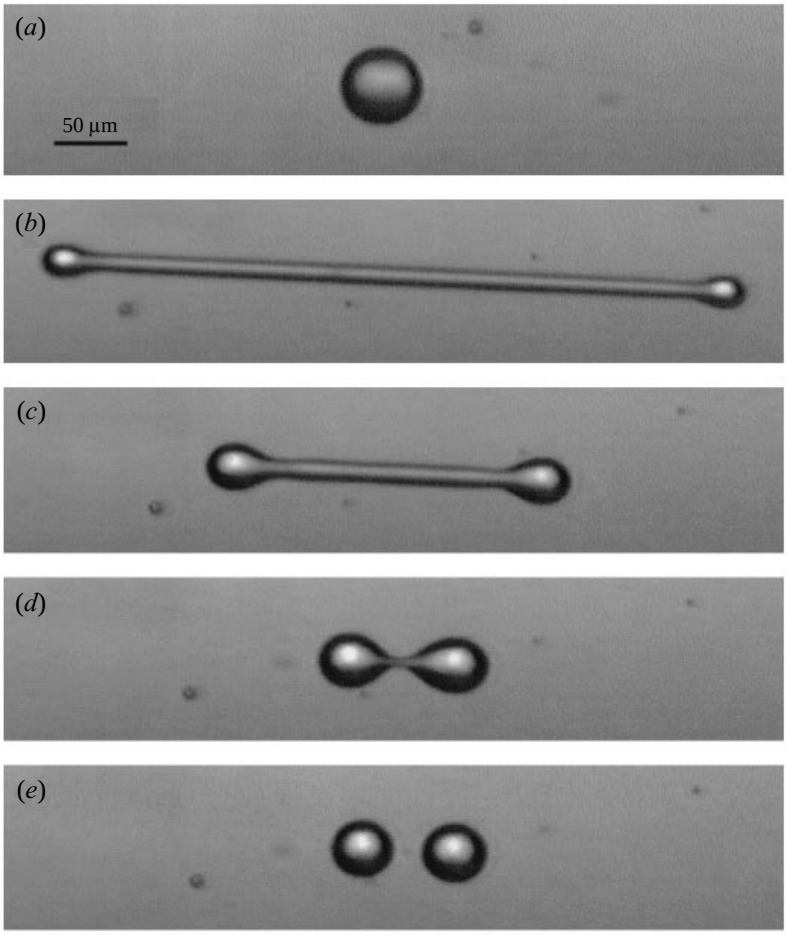


FIGURE 2. Break-up of a sheared drop after stopping the flow. (*a*) Drop at rest; (*b*) drop extended by shear; (*c*) and (*d*) drop retraction after stopping the flow; (*e*) the two drops generated by break-up.

could be controlled by further shearing the relaxing drop, either in the same sense or in the opposite sense with respect to the previously applied flow, as needed to prevent formation of multiple satellites. In such a way, it was possible to generate two daughter drops of about the same radius (ranging from 20 μm to 80 μm), with, at most, one tiny satellite in between them. The difference between the radii of the two drops was a few per cent of the average value.

Drop size was small enough to minimize wall effects. It is known from theoretical studies and numerical simulations that, for an isolated drop, the effect of a wall is to generate a migration away from the wall, a slip velocity parallel to the wall, and an increase of drop deformation (Chan & Leal 1979; Kennedy, Pozrikidis & Skalak 1994; Uijttewaal & Nijhof 1995). Such effects are a decreasing function of the ratio H/R, where H is the distance of the drop from the closer wall. The effects become negligible for H/R around 5, a condition which is fulfilled in the experiments presented in this work.

An aspect of the break-up process which was essential for this study was that, as a result, there was always a small, yet non-zero distance between the centres of the two daughter drops along the velocity gradient direction. This can be explained in the

https://doi.org/10.1017/S0022112097007921 Published online by Cambridge University Press

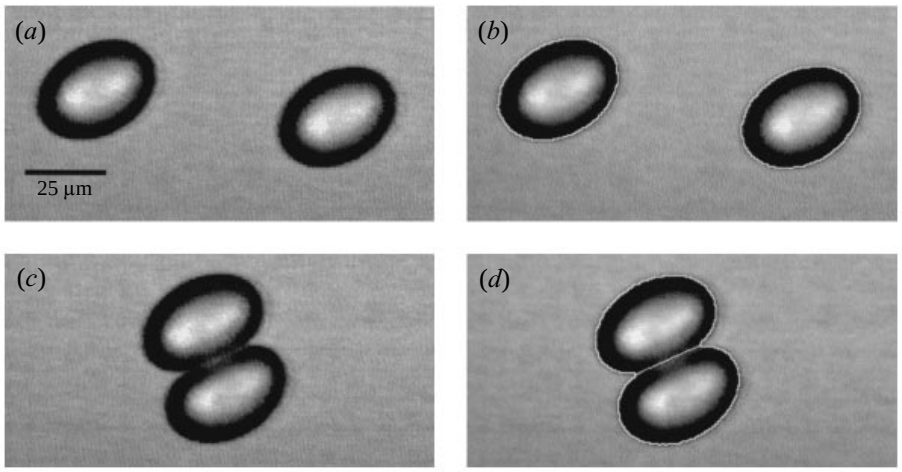


FIGURE 3. (*a*) Digital image of two drops during approach; (*b*) same image as in (*a*), drop contours as identified by image analysis are shown in white; (*c*) image of two colliding drops in close contact; (*d*) same image as in (*c*), the contours of the two drops have been separated and are drawn as white lines. $Ca = 0.13$, $\lambda = 1.4$, $R = 17$ μm.

following way. It is well known that the long axis of a drop under shear flow makes a certain angle (between 45° and 90°) with respect to the velocity gradient direction (Taylor 1934). Therefore, once the flow is stopped, the extended drop starts relaxing by forming two bulbous ends that are separated by a certain distance along the velocity gradient direction. Even though such distance is decreased by retraction, a small separation, of the order of a few tenths of the daughter drops radius, is still retained after break-up. The whole process is illustrated by the sequence of images presented in figure 2.

After break-up of the original drop, a shear flow was applied (keeping *Ca* below the critical value) in such a way as to further separate the two generated drops along the flow direction. Once the desired distance along the flow direction was reached, the shear was stopped and the drops were allowed to relax back to the spherical shape. The flow direction was then reversed and images of the drops during approach, collision and separation were recorded on video tape for later analysis, as will be described in the next subsection.

2.3. *Image analysis and data reduction*

A preliminary step for image analysis was to digitize a certain number of images of the colliding drops from the sequence recorded on video tape. Digitization was performed by means of a frame grabber (DT2867-LC, Data Translation), installed on a Pentium-based personal computer. The frame grabber was operated through image processing and analysis software (Global Lab Image, Data Translation). Image contrast was enhanced prior to digitization by adjusting gain and offset of the incoming video signal, which was then converted into an array of integers, ranging from 0 to 255, displayed on a monitor as grey levels. Digitization of images at consecutive times was performed in an automated way by running an especially-developed C-language macro which controlled frame grabber operation and stored images on hard disk in a compressed format. The time interval between successive images, which was given as input to the C macro, was set to either 2 or 3 s. A typical digital image of two drops during approach is presented in figure 3(*a*) ($Ca = 0.13$, $\lambda = 1.4$).

https://doi.org/10.1017/S0022112097007921 Published online by Cambridge University Press

Once a sequence of images was stored on hard disk, images analysis was performed by a second C macro calling some standard routines from the image analysis software library. Each image of the sequence was first averaged to reduce noise, then a grey level threshold was imposed to binarize the image while preserving continuity of drop contours. As an example, the contours of the drops of figure 3(*a*) are shown in figure 3(*b*). When the drops came into apparent contact, as exemplified in figure 3(*c*), their images looked merged together in the region of close approach and it was not possible to separate the two contours by a simple thresholding method. Instead, an algorithm based on boundary analysis was applied to the contour of the apparently merged drops. The two cusps corresponding to the extremes of the region of apparent contact were identified by analysing boundary curvature. As shown in figure 3(*d*), a white segment was drawn on the image between the two points, thus allowing separation of the two drops by the thresholding method described above.

The two drops were identified as objects in the binary image and the first and second moments of area along x and y were measured. A bilinear transformation (Gonzales & Woods 1992) was used to correct the moments of area for distortions introduced by the video camera. The coefficients of the transformation were preliminarily determined by using calibration graticules (Graticules Ltd). The two drop axes in the (x, y)-plane and the angle θ between the major drop axis and the y-direction were calculated from the corrected moments of area on the assumption of elliptical shape for the drop projection in the x, y-plane.

3. Results and discussion

This section is organized as follows. The application of the above described methodology to a typical collision experiment is presented in Section 3.1. The effect of Ca, λ and the initial separation between the two drops is described in Section 3.2. A comparison between experimental results and numerical simulations and theories from literature is made in Section 3.3.

3.1. *Standard collision experiment*

The reference system which will be adopted to describe the results is shown in figure 4. The coordinate frame is centred on the slower drop (i.e. the one closer to the fixed plate), which will be denoted as drop 1. The coordinate axes are oriented as follows: the x-axis is parallel to flow direction, the y-axis is parallel to the velocity gradient and points to the moving plate, and the z-axis is parallel to the vorticity direction. The relative trajectory of the two drops will be expressed in terms of the differences $\Delta y = y_2 - y_1$ and $\Delta x = x_2 - x_1$, where x_i and y_i are the centre-of-mass coordinates of the ith drop. It can be noticed that, with our choice of the reference system, the initial values of Δx and Δy are always negative and positive, respectively. The difference Δz between the z-coordinates of the two drops is close to zero, as a result of the drop formation technique described in the experimental section (Δz would be exactly zero in absence of any experimental imperfection, such as some residual misalignment). Since the drops are of slightly different size and almost neutrally buoyant, no significant increase of Δz owing to different settling velocities is expected in the time course of an experiment, which is of a few minutes.

In all the subsequent plots, Δx and Δy will be made dimensionless by using the average radius R of the undeformed drops as the characteristic length. In the collision experiment presented in this subsection, Ca was equal to 0.13 and λ was equal to 1.4 (PDMS was the inner phase). The difference between the radii of the two drops at rest

https://doi.org/10.1017/S0022112097007921 Published online by Cambridge University Press

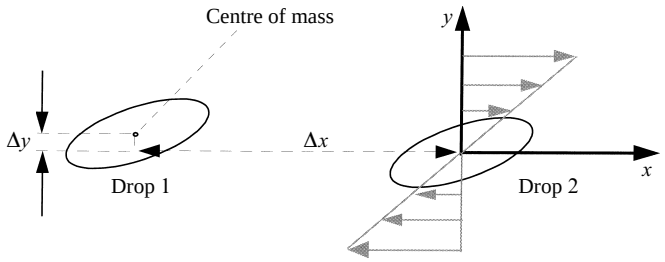


FIGURE 4. Frame of reference used to represent collision data.

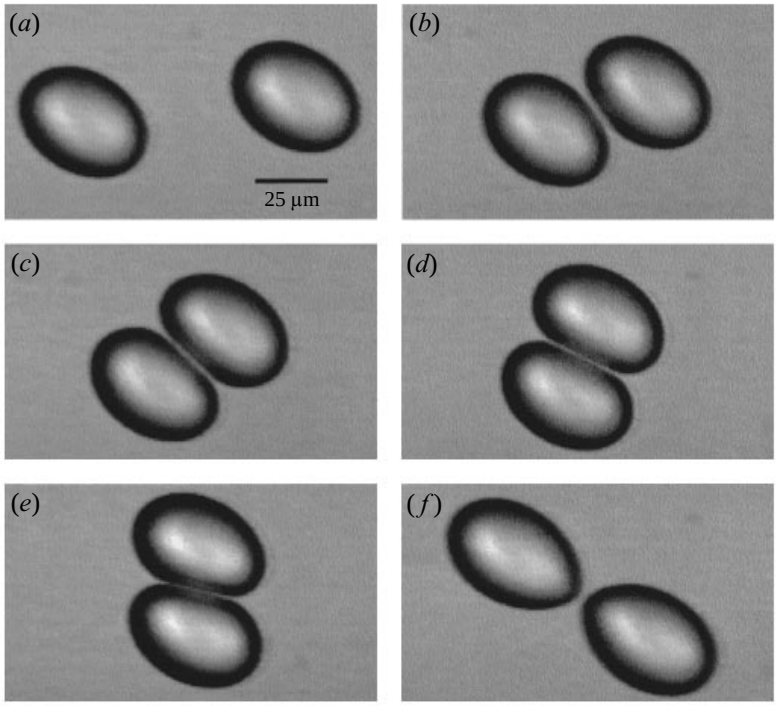


FIGURE 5. Sequence of images recorded in the course of a typical collision. $Ca = 0.13$, $\lambda = 1.4$, $R = 20$ μm.

was less than 1% of the average value, which was 20 μm. The gap size was about 675 μm and the shear rate was set at 0.21 s^{-1}. The drop Reynolds number was of the order of 10^{-7}, thus showing that inertial effects are negligible.

A sequence of six images of the colliding drops at successive times is shown in figure 5. In figure 6, Δy is plotted as a function of Δx during approach, collision and separation between the two drops. The data points corresponding to the images of figure 5 are indicated by arrows. It can be seen that Δy starts increasing after the drops come into apparent contact ($\Delta x \sim -2R$), goes through a maximum, and, after separation, reaches a new steady-state value. The trend was quite reproducible when the initial values of Δx and Δy were close to those of figure 6. However, for higher values of Δx, as will be discussed in the next section, Δy passed through a minimum when the two drops were approaching each other, the other qualitative features of the plot remaining the same.

https://doi.org/10.1017/S0022112097007921 Published online by Cambridge University Press

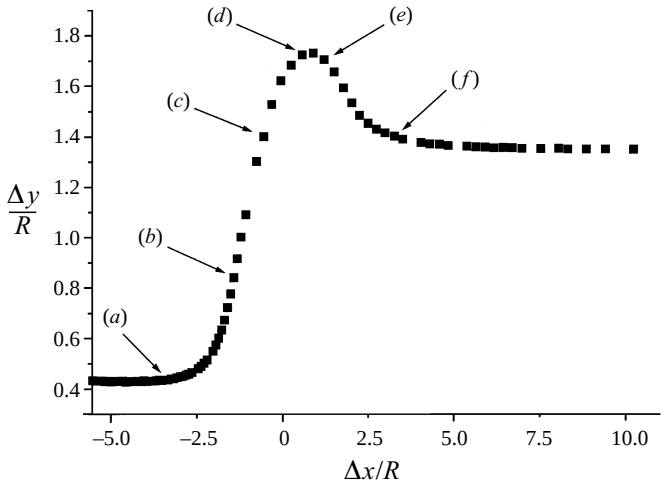


FIGURE 6. Plot of $\Delta y/R$ *vs.* $\Delta x/R$, same experiment as in figure 5.

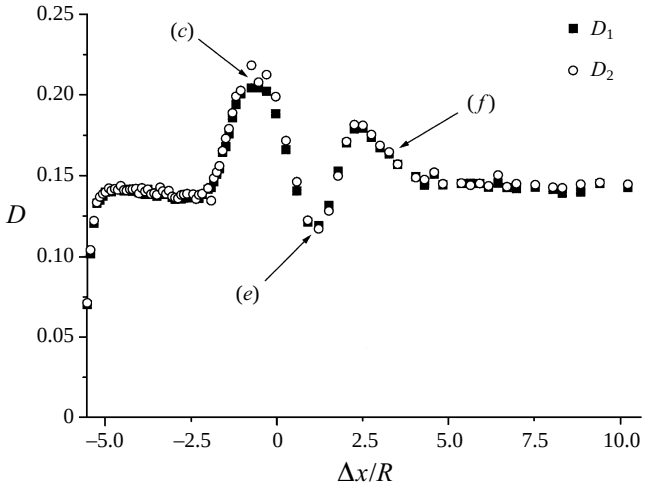


FIGURE 7. Plot of the deformation parameter D as a function of $\Delta x/R$, same experiment as in figure 5.

One of the most interesting aspects of figure 6 is that the final value of Δy, which is 1.35, is greater than the value before collision, which is 0.43. In fact, it was observed that, if the drops were made to collide again by reversing the flow direction, Δy increased further. In other words, the effect was irreversible, and repeated collisions led to increasing values of Δy until drop interaction became negligible. This result extends the work by Mason's group (Bartok & Mason 1959; Allan & Mason 1962), which was restricted to quasi-spherical drops, and is in agreement with the numerical simulations of Loewenberg & Hinch (1996*a*, *b*), who investigated also the case of significantly deformed drops.

In figure 7 the deformation parameters D_1 and D_2 of the two drops are plotted as a function of Δx. In the following, the deformation parameter of either drop will be designated as D, since the two sets of data appear to coincide within the experimental error (including the small difference in size between the drops). D slightly decreases during approach, then goes through a maximum (point (*c*)), a minimum (point (*e*)), a

https://doi.org/10.1017/S0022112097007921 Published online by Cambridge University Press

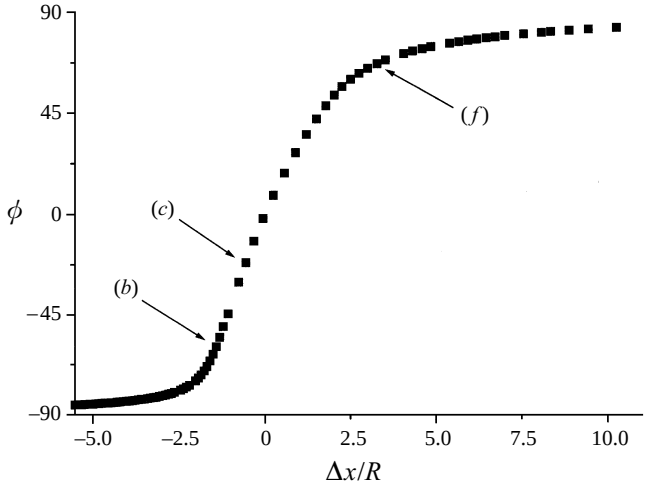


FIGURE 8. Plot of the angle λ between the line joining drop centres and x-axis *vs.* $\Delta x/R$, same experiment as in figure 5.

second maximum, and eventually reaches a steady state at the same constant value as before the collision. It should be pointed out that such a steady-state value of D, corresponding to isolated drop behaviour, is attained shortly after start-up of the experiment. It follows that the drops reach a stationary shape long before they interact, thus ensuring that the collision is not affected by transient effects during start-up.

The trend displayed by the deformation parameter can be explained in a qualitative way by regarding the two drops, while they are in close contact, as forming a single object, or, more precisely, a 'collision doublet', following Allan & Mason (1962). The orientation of the doublet can be expressed by introducing the angle ϕ that the line joining the centres of mass of the two drops makes with respect to y-axis. The plot of ϕ as a function of Δx is presented in figure 8. The limiting values of ϕ are $-90°$ for $\Delta x \to -\infty$ and $+90°$ for $\Delta x \to +\infty$, the trend of ϕ being sigmoidal in between.

The force exerted by the surrounding fluid on the doublet will act to push the two drops together in the compressional quadrant of shear flow (where $\phi < 0$). It follows that the deformation parameter of each drop increases in the compressional quadrant and this trend is shown by both the sequence in figure 4 (images (*b*) and (*c*)) and the plots of figure 7 (up to the first maximum, point (*c*)). When the doublet reaches the extensional quadrant, the deformation parameter starts decreasing and reaches a minimum (point (*d*) in figure 7 and corresponding image in figure 4). The minimum value of D is lower than the steady-state value before (or after) collision. Such a decrease of D can be explained as the result of two processes: (i) relaxation of drop shape once the doublet leaves the compressional quadrant, and (ii) action of the surrounding fluid on the drops. In the latter process, the surrounding fluid exerts an extensional force on the doublet, which is now oriented along an angle ϕ lower than the angle θ of either drop (the plot of θ *vs.* Δx will be presented in the following paragraph). It follows that the force experienced by each drop acts to decrease the deformation. Upon increase of ϕ in the course of collision, the orientation of the doublet gets closer to the orientation of either drop. The extensional action of the surrounding fluid leads now to an increase of D up to a maximum when the drops separate. The two drops then relax to the steady state shape in the absence of interaction.

https://doi.org/10.1017/S0022112097007921 Published online by Cambridge University Press

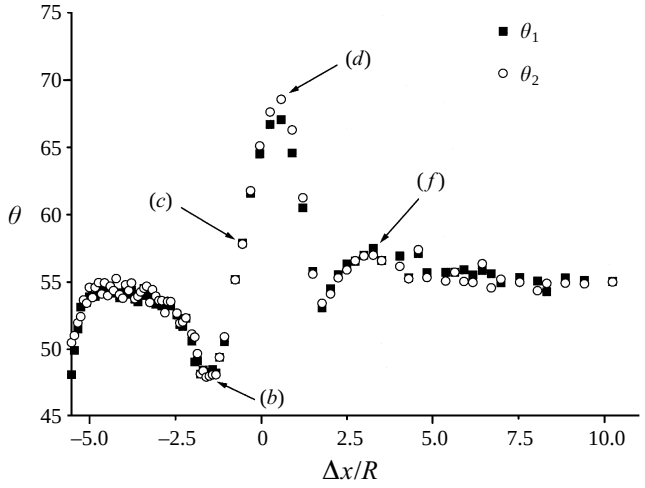


FIGURE 9. Plot of the angle θ between drop major axis and velocity gradient direction *vs.* $\Delta x/R$, same experiment as in figure 5.

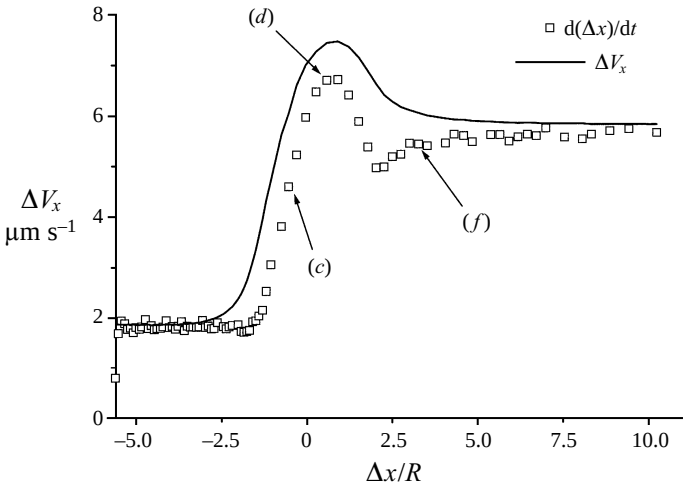


FIGURE 10. Plot of the relative velocity ΔV_x between the drops in the x-direction *vs.* $\Delta x/R$, same experiment as in figure 5. The continuous line has been calculated as $\dot{\gamma}\Delta y$.

A similar oscillatory trend is displayed by the angle θ that either drop makes with respect to the y-axis, as shown in figure 9. The main differences are that (i) θ goes first through a pronounced minimum (shown by arrow 2 in figure 9) at $\Delta x \sim -1.6$, whereas D only slightly decreases in this interval of Δx, and (ii) the two maxima of θ lag behind those of D. The decrease of θ pointed out in (i) starts when the two drops come into contact and are pushed against each other in the compressional quadrant of shear flow. At some point, while the drops are sliding over each other, the trend is reversed and the drops become more oriented along the flow direction, as shown by images 3 and 4 of figure 5. A similar qualitative description can be applied to the behaviour of θ in the extensional quadrant of shear flow.

In figure 10 the relative velocity between the centres of mass along the flow direction, indicated as Δv_x, is plotted as a function of Δx. Δv_x has been calculated as $\mathrm{d}(\Delta x)/\mathrm{d}t$

https://doi.org/10.1017/S0022112097007921 Published online by Cambridge University Press

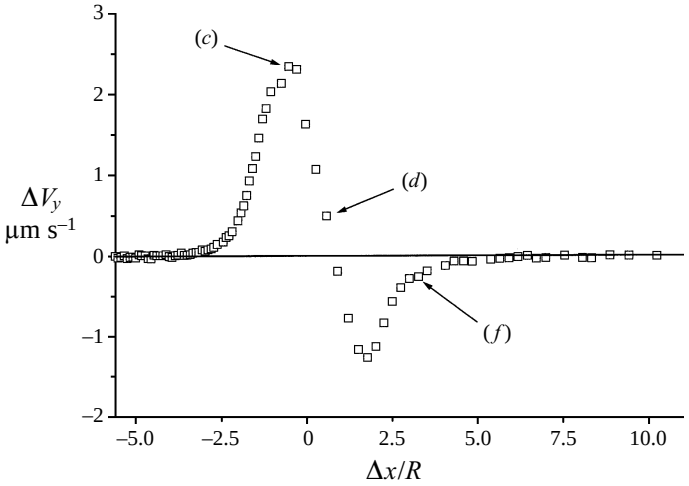


FIGURE 11. Plot of the relative velocity ΔV_y between the drops in the y-direction *vs.* $\Delta x/R$, same experiment as in figure 5.

from the experimental data and then plotted *vs.* Δx for comparison with the previous diagrams. It can be seen that Δv_x increases rapidly when the drops start interacting, thus showing that drops accelerate while sliding over each other. The final steady-state value of Δv_x is, of course, higher than the initial one, owing to the increased distance between the two drops along the y-axis. The continuous curve in figure 10 has been calculated as $\dot{\gamma}\Delta y$, with $\dot{\gamma} = 0.21\ \mathrm{s}^{-1}$ and Δy being the experimental value corresponding to each Δx. Therefore, the continuous curve represents the relative velocity between the centres of mass if the drops moved relative to the continuous phase. Before and after collision, the dashed curve actually coincides with the experimental data, whereas one drop retards the other during interaction.

The relative velocity along the velocity gradient Δv_y is plotted as a function of Δx in figure 11. The value of Δv_y before and after collision is zero, as expected. Δv_y is positive when the drops are sliding over each other and the distance between the centres of mass along y increases, and becomes negative when the drops are separating and the increase in Δy is partly recovered.

3.2. *Effect of Ca and λ*

As mentioned in the previous section, in some experimental conditions Δy went through a minimum before the drops came into apparent contact. An example of a plot of Δy *vs.* Δx with such a minimum will be presented in the following (figure 13). The presence of a minimum indicates that the drops move towards each other along the velocity gradient direction. To exclude experimental artifacts, the trend of the y-coordinate of each drop during approach was examined. It was verified that y_1 and y_2 are, respectively, a decreasing and an increasing function of Δx, thus showing that the drops actually move towards each other during approach. The minimum was observed only when the initial separation between the drops along the x-axis was greater than about 6 times the undeformed radius. The value of Δx corresponding to the minimum was around -3. The depth of the minimum was dependent on the capillary number: the higher the value of Ca, the deeper the minimum. In some cases, the value of Δy went so close to 0 that the drops did not collide in the course of the experiment, even at the highest total strain allowed by the apparatus.

https://doi.org/10.1017/S0022112097007921 Published online by Cambridge University Press

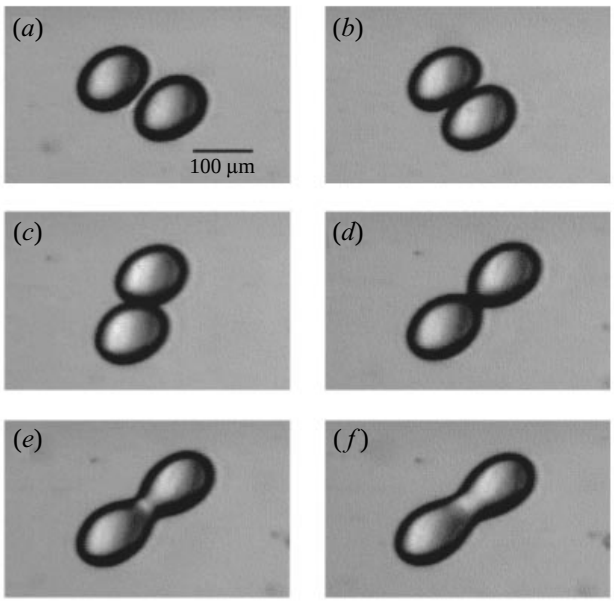


FIGURE 12. Sequence of images showing a collision with coalescence. $Ca = 0.13$, $\lambda = 0.36$.

Apart from the influence on the minimum of Δy, the effect of Ca in the range investigated (0.07–0.36) can be described as follows. Both the maximum value of Δy and the corresponding value of Δx showed a slight increase for decreasing values of Ca. A possible explanation of such a trend is that with decreasing Ca the drops are less deformed and so act as bigger obstacles for each other. The final steady-state value of Δy varied from 1.2 to 1.3 and no significant trend could be inferred from the data beyond the scatter due to experimental error. The behaviour of D and θ was also qualitatively similar in the range of Ca investigated.

The effect of λ was evaluated by changing the PDMS sample used as the drop fluid. The viscosity ratio was 1.4 for PDMS 100 and 2.0 for PDMS 200. The trend of Δy, D and θ was qualitatively similar in the two cases. The final value of Δy after collision did not exhibit a significant variation, either.

Coalescence was not observed in any of the experiments described so far. As mentioned in §2.1, some experiments were also carried out by using PIB as the fluid phase. The results can be taken as only qualitative, since the actual value of the viscosity ratio at the time of collision is different from the initial one owing to diffusion of PIB in PDMS. In such experiments, coalescence, though a rare event, was observed in a few cases and it took place in the extensional quadrant of shear flow, when the drops were about to separate.

An example is shown in the sequence of images presented in figure 12. The drop formed from coalescence was broken again and a new collision experiment was performed, at the same Ca (0.13). In such a case, however, drop interaction did not lead to coalescence. In figure 13, Δy is plotted *vs.* Δx for the two successive experiments just described. Apart from the different paths followed during the approach, owing to the different initial separations between the drops in the two experiments, the plots of figure 13 coincide until coalescence. It follows that the different behaviour observed in the two experiments cannot be attributed to a difference in drop kinematics. A possible explanation is the progressive accumulation of impurities at the interface in the course

https://doi.org/10.1017/S0022112097007921 Published online by Cambridge University Press

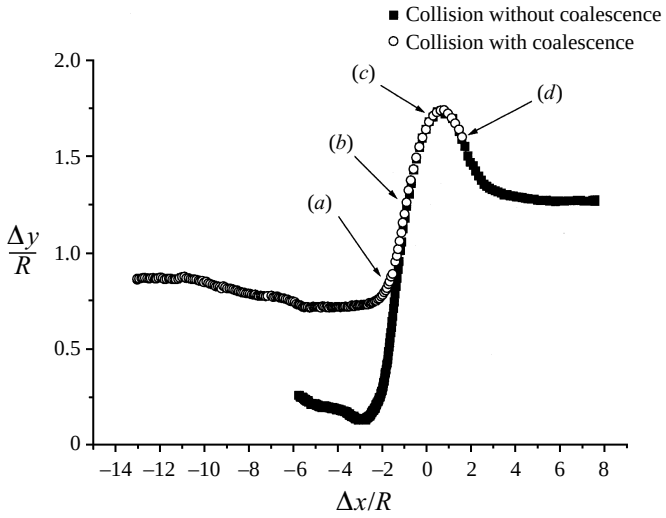


FIGURE 13. Plot of $\Delta y/R$ *vs.* $\Delta x/R$ for $Ca = 0.13$, $\lambda = 0.36$. The circles (○) correspond to the collision with coalescence of figure 12. The squares (■) correspond to a collision between two drops generated by break-up of the drop formed upon the coalescence shown in figure 12.

of the experiments, leading eventually to inhibition of coalescence. Such interpretation has already been proposed to explain the lack of reproducibility in coalescence experiments where a drop was made to contact a flat liquid interface by gravity (Charles & Mason 1960). Another explanation is a possible effect of the diffusion of PIB from the drops in the continuous phase. However, according to the results of MacKay & Mason (1964), the diffusion of a component out of the drops inhibits coalescence.

3.3. *Comparison with theories and numerical simulations in literature*

As mentioned in §1, Allan & Mason (1962) developed a simplified model for the collision of two equi-sized drops in simple shear flow. The model is restricted to the case of quasi-spherical drops, i.e. only slightly deformed by shear flow. Van der Waals force of attraction was not taken into account by Allan & Mason, but it was included in the extension of the model developed by Jeelani & Hartland (1993). The two drops in near contact were described as a collision doublet of ellipsoidal shape, on which the suspending fluid generates a force along the major axis given by Jeffery's generalized theory for rigid ellipsoids. The axis ratio r_e of the doublet was assumed equal to 2 and doublet orientation was described by the angle ϕ. The compressional force at $\phi < 0$ acts to push the two drops together and to flatten them in the apparent contact region. By assuming instantaneous response to the compressional force, the following expressions were obtained for the radius c of the apparent contact region

$$\frac{c}{R} = (2.17Ca \sin(-2\phi))^{1/2} \quad \text{for } \phi < 0, \tag{1}$$

$$c = 0 \quad \text{for } \phi > 0. \tag{2}$$

Based on such expressions for c, an equation was then derived for the velocity of approach of the two drops, which was integrated to calculate Δy as a function of Δx. The model predicts that the steady-state value of Δy after collision is greater than the initial one.

https://doi.org/10.1017/S0022112097007921 Published online by Cambridge University Press

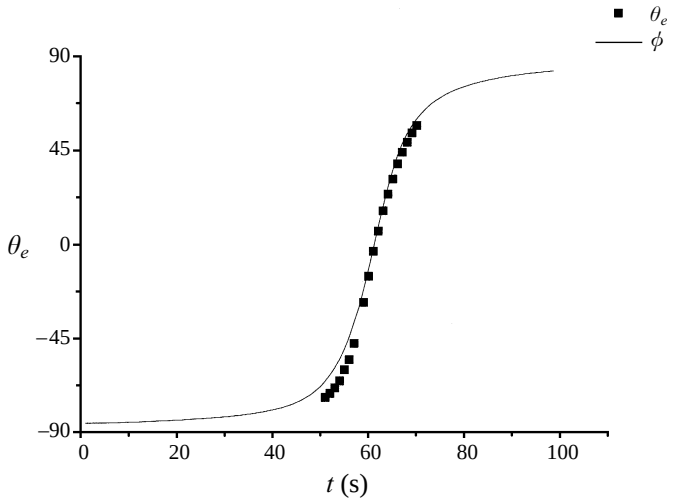


FIGURE 14. Plot of ϕ *vs.* time (continuous line), and of θ_e, the angle between doublet major axis and y-direction, *vs.* time (full squares).

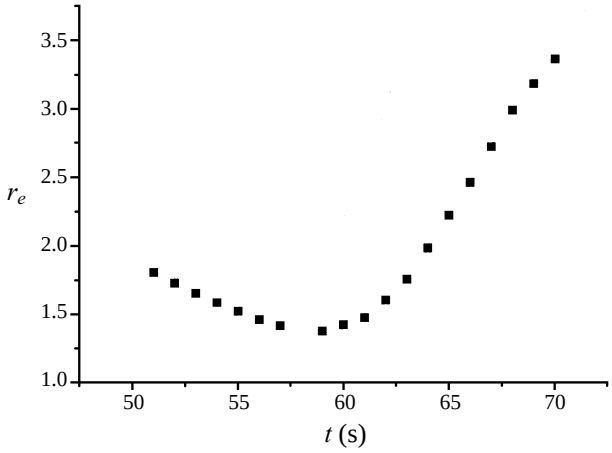


FIGURE 15. Plot of the axis ratio of the doublet r_e as a function of time.

To evaluate whether the Allan & Mason model can be used to describe the collision data presented in this work, the images of the drops in close contact, i.e. when they can be described as a collision doublet, were analysed without using an algorithm to separate the two drops. The moments of area of the doublet were measured and the axis ratio r_e and the angle θ_e of the equivalent ellipse were calculated, as described in §2.3. Typical plots of θ_e *vs.* time and of r_e *vs.* time are presented in figures 14 and 15, respectively. In figure 14, the plot of ϕ (defined, as in §3.2, as the angle between the line joining the centres of mass of the two drops and the y-axis) *vs.* time is also shown as a continuous line. The good agreement between ϕ and θ_e shows that both the methods of calculating the doublet angle lead essentially to the same results. The plot of figure 15 shows that r_e assumes values between 1.4 and 3.3, with an average of 2.0, which is the value considered by Allan & Mason for quasi-spherical drops.

So far, the model by Allan & Mason gives a reasonable description of drop collision even for significantly deformed drops. To test model predictions, the extent c of the

https://doi.org/10.1017/S0022112097007921 Published online by Cambridge University Press

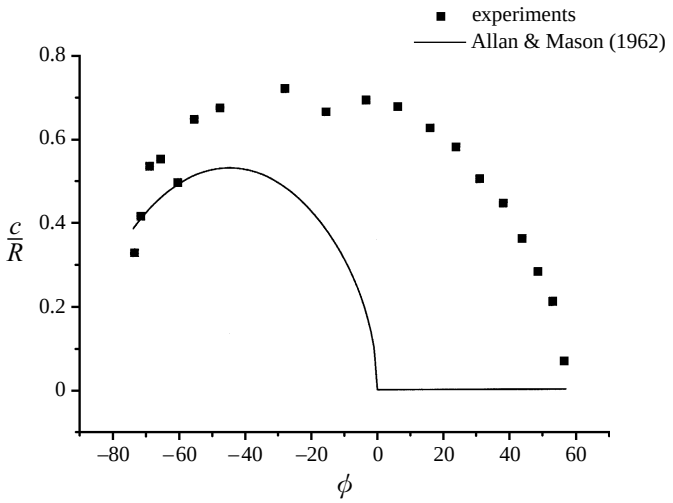


FIGURE 16. Plot of c/R, where c is the extent of the near-contact region, as a function of ϕ. The squares are experimental data; the continuous line corresponds to the Allan & Mason model (1962).

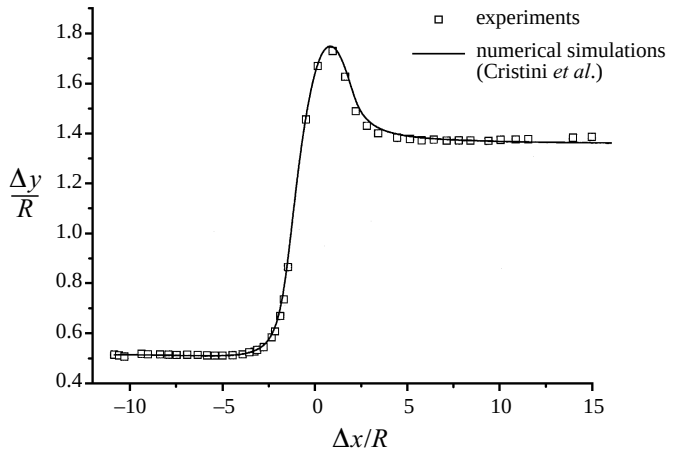


FIGURE 17. Comparison between experiments and numerical simulations by Cristini *et al.* (unpublished work). The open squares are experimental data of $\Delta y/R$ *vs.* $\Delta x/R$, the continuous line is the numerical simulation. $Ca = 0.135$, $\lambda = 1.37$.

apparent contact region was estimated from the images of the colliding drops. As described in §2.3, the extremes of the near contact region were taken as the two cusps on the contour of the apparently merged drops. A plot of the estimated c value as a function of ϕ is presented in figure 16 for a collision at $Ca = 0.13$ and $\lambda = 1.4$. The continuous line in figure 16 represents equation (1). The main difference between the theoretical curve and the data is that the near contact region experimentally observed does not reduce to a point at $\phi = 0$, as assumed by the Allan & Mason model. Such a difference does not depend on the way c was estimated in this work, being immediately evident from the unprocessed images. The discrepancy was pointed out by Allan & Mason for the case of quasi-spherical drops and was attributed to a relaxation effect not taken into account by the model, which is based on instantaneous response to the force exerted on the doublet by the suspending fluid. No further attempt of

https://doi.org/10.1017/S0022112097007921 Published online by Cambridge University Press

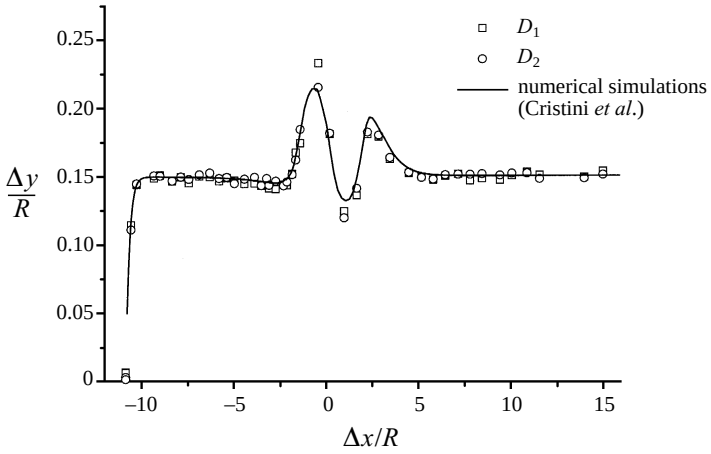


FIGURE 18. Comparison between experimental and numerical values of the deformation parameter D *vs.* $\Delta x/R$. The squares and the circles correspond to the deformation parameters D_1 and D_2 of the two drops, the continuous line is the numerical simulation (Cristini *et al.* unpublished work). Same conditions as in figure 17.

comparison with the Allan & Mason model was made, since the fundamental equation derived for the velocity of approach of the two drops involves a quantity, i.e. the distance between the drop surfaces, which was not resolvable in the near-contact region by the optics used in this work.

Numerical simulations of collisions between two drops in shear flow have been recently reported by Loewenberg & Hinch (1996*a*, *b*), as mentioned in §1. All the qualitative features of binary collisions observed in this work are in agreement with the numerical simulations. In particular, the minimum in the plot of Δy *vs.* Δx is also present in the results presented by Loewenberg & Hinch (1996) and gets more pronounced with increasing Ca. A quantitative comparison between experimental results obtained in this work and calculations kindly performed ad hoc by Loewenberg and co-workers (V. Cristini, J. Blawzdziewicz & M. Loewenberg, unpublished work) is presented in figures 17 and 18.

In figure 17, Δy is plotted as a function of Δx for $Ca = 0.135$ and $\lambda = 1.37$. The continuous lines represent numerical simulations, while the open squares correspond to the experimental data. The numerical simulations were performed using the same initial values of Δx and Δy as in the experimental data presented in figure 17, Δz was set to 0. The comparison shows a good agreement between experiments and numerical simulations. Van der Waals attraction was not taken into account in the numerical simulations. In fact, it is unlikely that van der Waals forces are strong enough to bias drop trajectories without leading to coalescence.

Numerical and experimental data of D *vs.* Δx are compared in figure 18, for the same two experiments presented in figure 17. The agreement is again quite good, both from the qualitative and quantitative point of view. Numerical and experimental results show the same qualitative features, and the only significant quantitative difference is in the value of the first maximum of D, which is higher in the numerical simulations. The discrepancy can be attributed to approximations in the determinations of D in the near contact region, both in the numerical simulations and in the experimental data. The latter correspond to an ellipse equivalent in area to the actual drop, whereas in the near-contact region some deviations from elliptical shape are expected (though modest), given the flattening at the interface. As pointed out by Loewenberg & Hinch

https://doi.org/10.1017/S0022112097007921 Published online by Cambridge University Press

(1996*a*), numerical simulations, on the other hand, tend to over-predict drop deformation due to surface discretization. The two sources of error go in opposite directions, since the experimental error acts to underestimate the deformation parameter, while the numerical approximations act to overestimate it.

4. Concluding remarks

In this work, a methodology to study collisions between two drops in shear flow has been developed. The colliding drops have been observed along the vorticity direction of shear flow by video-enhanced contrast optical microscopy. Image analysis techniques have been applied to measure the relative trajectory of the drops and to characterize the deformation experienced by each drop in the course of collision. One of the features observed studying relative trajectories is that collision always acts to separate further the two drops along the velocity gradient direction. In a concentrated system (e.g. a polymer blend or an emulsion), such an effect leads to a shear-induced self-diffusion of drops, which has been studied by Loewenberg & Hinch (1996*b*) through numerical simulations. On the assumption that the system is so dilute that only pairwise interactions need to be considered, these authors found that self-diffusion is anisotropic, being much larger in the velocity gradient direction than in the vorticity direction. An experimental estimate of the corresponding two self-diffusion coefficients cannot be made by using the results of this work, since the dependence of trajectory displacement of Δz has not been investigated. Work on this aspect is in progress.

Coalescence has been observed when the drops were about to separate, in agreement with the predictions of Loewenberg & Hinch (1996*b*), based on scaling arguments. The lack of reproducibility which was observed in two subsequent collisions was attributed to accumulation of impurities at the interface. It should be pointed out that this is only a tentative explanation based on similar results reported in the literature, since a full understanding of the coalescence process has not yet been reached. A quantitative comparison with coalescence models presented in the literature (Chester 1991) was not possible, since it requires data for the thickness of the film between the drops. Such data could not be obtained in this work, as the distance between the surfaces of colliding drops in the near contact region was not resolvable with the optics used.

Good agreement was found between experimental data obtained in this work and numerical simulations in the literature (Loewenberg & Hinch, 1996*a*, *b*; Cristini *et al.* unpublished work). The minimum observed in the plot of Δy *vs.* Δx is also present in the simulations. Furthermore, the dependence of the minimum on Ca and on the initial value of Δx is correctly predicted. This work has been restricted to values of Δz close to 0. A knowledge of the dependence of trajectory displacement on Δz would allow a more accurate comparison with numerical simulations. Work is in progress in this area.

Financial support by the European Community under the BRITE-EURAM contract BRE2.CT 920213 is gratefully acknowledged. The authors are indebted to Dr Michael Loewenberg and coworkers for kindly performing numerical simulations to be compared with experimental data and for helpful discussions. The authors wish to thank Professor Giuseppe Marrucci for critical reading of the manuscript and valuable advice. Helpful remarks and suggestions from Dr Francesco Greco are gratefully acknowledged.

https://doi.org/10.1017/S0022112097007921 Published online by Cambridge University Press

REFERENCES

Allan, R. S. & Mason, S. G. 1962 Particle motion in sheared suspensions. XIV. Coalescence of liquid drops in electric and shear fields. *J. Colloid Sci.* **17**, 383–408.

Bartok, W. & Mason, S. G. 1957 Particle motions in sheared suspensions. V. Rigid rods and collision doublets of spheres. *J. Colloid Sci.* **12**, 243–262.

Bartok, W. & Mason, S. G. 1959 Particle motion in sheared suspensions. VIII. Singlets and doublets of fluid spheres. *J. Colloid Sci.* **14**, 13–26.

Chan, P. C.-H. & Leal, L. G. 1979 The motion of a deformable drop in a second-order fluid. *J. Fluid Mech.* **92**, 131–170.

Charles, G. E. & Mason, S. G. 1960 The coalescence of liquid drops with flat liquid/liquid interfaces. *J. Colloid Sci.* **15**, 236–267.

Chesters, A. K. 1991 The modelling of coalescence processes in fluid–liquid dispersions: a review of current understanding. *Trans. I. Chem. E.* **69**, 259–270.

Eckstein, E. C., Bailey, D. G. & Shapiro, A. H. 1977 Self-diffusion of particles in shear flow of a suspension. *J. Fluid Mech.* **79**, 191–208.

Gonzales, R. C. & Woods, R. E. 1992 *Digital Image Processing*, pp. 61–68, Addison-Wesley.

Jeelani, S. A. K. & Hartland, S. 1993 Effects of velocity fields on binary and interfacial coalescence. *J. Colloid Interface Sci.* **156**, 467–477.

Kennedy, M. R., Pozrikidis, C. & Skalak, R. 1994 Motion and deformation of liquid drops, and rheology of dilute emulsions in simple shear flow. *Comput. Fluids* **23**, 251–278.

Leighton, D. T. & Acrivos, A. 1987 Measurement of shear-induced self-diffusion in a concentrated suspension of spheres. *J. Fluid Mech.* **177**, 109–131.

Loewenberg, M. & Hinch, E. J. 1996*a* Numerical simulation of a concentrated emulsion in shear flow. *J. Fluid Mech.* **321**, 395–419.

Loewenberg, M. & Hinch, E. J. 1996*b* Collision of two deformable drops in shear flow. *J. Fluid Mech.* **338**, 299–315.

MacKay, G. D. & Mason, S. G. 1964 Particle motions in sheared suspensions. XV. Effects of diffusion on collision doublets of fluid drops. *Kolloid-Z.* **195**, 138–148.

Sigillo, I., di Santo, L., Guido, S. & Grizzuti, N. 1997 Comparative measurements of interfacial tension in a model polymer blend. *Polymer Engng Sci.* **37**, 1540–1549.

Taylor, G. I. 1934 The formation of emulsions in definable fields of flow. *Proc. R. Soc. Lond.* A **146**, 501–523.

Uijttewaal, W. S. J. & Nijhof, E. J. 1995 The motion of a droplet subjected to linear shear flow including the presence of a plane wall. *J. Fluid Mech.* **302**, 45–63.

https://doi.org/10.1017/S0022112097007921 Published online by Cambridge University Press